Field Measurements of Undertow on Longshore Bars

Yoshiaki KURIYAMA[1]

Abstract

Field measurements of undertow over longshore bars were conducted at Hazaki Oceanographical Research Station (HORS) on the Kashima coast of Japan facing the Pacific Ocean. The field measurements, other field measurements and large-scale experiments were compared with one-dimensional models for undertow; one of them was developed in this study. The comparisons showed that the present model well predicted the undertow velocities over longshore bars in the field, while a previous model calibrated with small-scale experiment data underestimated the velocities.

1. Introduction

The prediction of undertow velocity over a longshore bar is required for predicting the deformation of the bar, which breaks waves and reduces the wave energy to protect the beach as a submerged breakwater. The undertow velocity prediction over a bar is also required for designing offshore nourishment, which has been recently developed in the United States, Australia and Europe (e.g., McLellan and Kraus, 1991); nourished sediment forms an artificial bar and the prediction of the bar movement is essential for the offshore nourishment project.

Although many models for undertow have been developed and verified with experiment data on planar beaches (e.g., Svendsen, 1984; Stive and Wind, 1986; Svendsen and Hansen, 1988; Okayasu et al. 1988; Deigaard et al., 1991; Dally and Brown, 1995), only a few models have been verified with data on barred beaches in experiments (Okayasu and Katayama, 1992; Rakha et al., 1996) and in the field (Smith et al., 1992; Haines and Sallenger, 1994). In this study, hence, field measurements of undertow were conducted over longshore bars at Hazaki Oceanographical Research Station (HORS) and compared with one-dimensional models for undertow, which predict the depth-averaged undertow velocity below the wave trough level; one of the models was developed in this

[1] Head, Littoral Drift Laboratory, Marine Environment Division, Port and Harbour Res. Inst.
Ministry of Transport, Nagase 3-1-1, Yokosuka, Kanagawa 239-0826, JAPAN
E-mail: kuriyama@cc.phri.go.jp

study. The models were also compared with other data obtained over longshore bars in large-scale experiments and in the field. The purposes of this paper are to describe the field measurements at HORS and to show the comparisons of undertow velocities measured and predicted.

2. Field Measurements

Field measurements were conducted from January 29 to February 3, 1997 at HORS, which is a field observation pier of 427 m in length on the Kashima coast of Japan facing the Pacific Ocean; the location of HORS is shown in Figure 1. Cross-shore and longshore current velocities were measured with electro-magnetic current meters for thirty minutes every two hours at a sampling frequency of 5 Hz, and water surface elevations were measured with ultrasonic wave gages. Wave breaking positions and types, and the locations of rip currents were visually observed several times a day, and the beach profile along HORS has been measured daily every 5 m.

The locations of the measurement points are shown in Figure 2 with the beach profiles on January 31 and February 1; the reference level is the Hasaki datum level, which is equal to the low water level, and the tidal rage is 1.4 m. Seaward bar migration occurred on January 31, and the bar crest moved seaward about 50 m. Except for the bar migration, no significant beach profile changes occurred during the measurements. The measurement point where the seaward distance is 230 m (referred to as P230m) was located shoreward of the bar crest, while the measurement point of P290m was located seaward of the bar crest. The measurement point of P260m was located just seaward of the bar crest before the bar migration and shoreward of the bar crest after the bar migration.
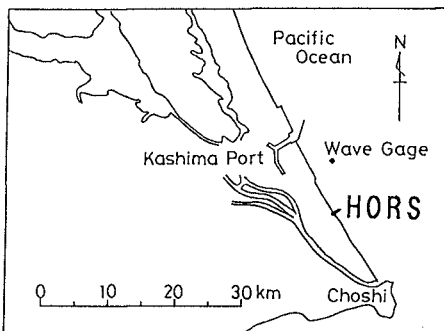
Figure 1   Location of HORS.
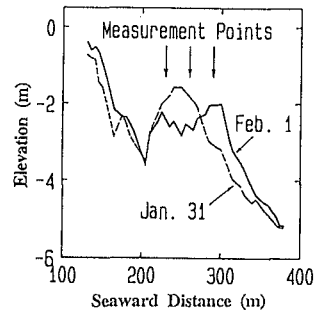
Figure 2   Locations of current meters and beach profiles on Jan. 31 and Feb. 1.

The seaward bar migration on January 31 damaged the supporting systems of the current meters at all measurement points, and current velocities were not measured temporarily. At P260m, two current meters were installed on January 29 at D.L. -0.87 m and D.L. -1.37 m, and were reinstalled on February 1 after the damage at D.L. -1.09 m and D.L. -1.59 m. At P230m, one current meter was installed at D.L. -1.99 m and reinstalled at D.L. -1.90 m. Although at P290m, a current meter was installed at D.L. -1.72 m, the supporting system of the current meter was completely destroyed at 7 a.m. on January 31, and then current velocities were not measured any more.

Figure 3 shows the time series of significant wave height $H_{1/3}$, significant wave period $T_{1/3}$ and undertow velocity V measured. The significant wave heights at the tip of HORS, where the water depth was approximately 6m, increased from 11 p.m. on January 30, reached about 2.6m at 8 a.m. on January 31, and then gradually decreased. Undertow velocities increased as the wave heights increased, and from February 1 fluctuated regardless of the wave height changes.

Nearshore currents during the measurements are considered to be uniform alongshore owing to two reasons mentioned below. First, in the visual observations conducted several times a day during the measurements, no rip currents were observed, and the breaker lines were linear alongshore. Second, the low-frequency components of cross-shore current velocities $v_{rms,l}$ (<0.04 Hz) were not related to the undertow velocities as shown in Figure
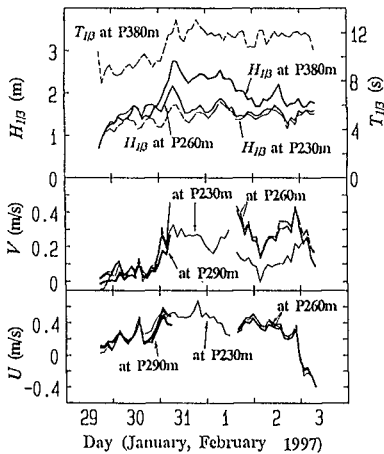
Figure 3 Time series of significant wave height $H_{1/3}$ and period $T_{1/3}$, and undertow velocity V.
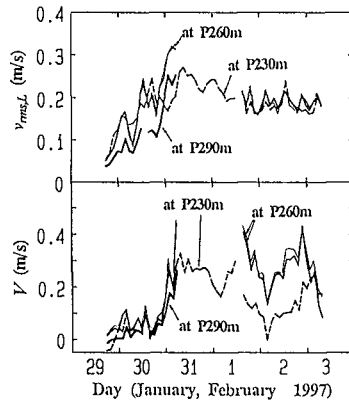
Figure 4 Time series of low-frequency component of cross-shore current velocity $v_{rms,l}$ and V.

4; the low-frequency components were relatively constant although the undertow velocities significantly changed. Some field measurements showed that rip currents were intermittent events (Wright and Short, 1983; Short, 1985; Smith and Largier, 1995), and hence the low-frequency component of cross-shore current in or near a rip current is expected to be large. The constant low-frequency components of the cross-shore currents in Figure 4 suggest that the possibility of rip current during the measurements is low.

3. Numerical Model

The one-dimensional model of undertow developed here consists of a wave transformation model and an undertow model, and adopts a wave-by-wave approach, in which wave heights and undertow velocities are calculated for individual waves. The time-averaged undertow velocity for an irregular wave group is estimated with averaging the undertow velocities of individual waves weighted according to the wave periods.

3-1 Wave transformation model

The wave transformation model is based on the model developed by Kuriyama (1996). The shoaling of a wave is estimated with a shoaling coefficient proposed by Shuto (1974) with the consideration of wave nonlinearity.

The criterion on wave breaking is based on a formula proposed by Seyama and Kimura (1988). Because Seyama and Kimura (1988) proposed the formula on the basis of experimental data, Kuriyama (1996) introduced a dimensionless coefficient C_{br} to adjust the formula to field data. The criterion is expressed by the following equation with the wave height-water depth ratio at wave breaking H_b/h_b, wavelength in deep water L_0, and beach slope $\tan\beta$, which is defined here as the average slope in the area from 15 m shoreward of the definition point to 15 m seaward of the point.

$$\frac{H_b}{h_b} = C_{br}\left[0.16\frac{L_0}{h_b}\left[1 - \exp\left\{-0.8\pi\frac{h_b}{L_0}(1 + 15\tan^{4/3}\beta)\right\}\right] - 0.96\tan\beta + 0.2\right]. \quad (1)$$

Energy dissipation of a wave in the surf zone is estimated with a periodic bore model used by Thornton and Guza (1983); the model is expressed by

$$\frac{\partial E_w C_g}{\partial y} = \frac{1}{4}\rho g\frac{1}{T}\frac{(BH)^3}{h}, \quad (2)$$

where E_w is the energy of wave motion, C_g is the group velocity, ρ is the sea water density, T is the wave period, H is the wave height, h is the water depth, and B is a dimensionless coefficient determining the amount of energy dissipation. Kuriyama and Ozaki (1996) investigated the coefficient B with the experiment data of Seyama and Kimura (1988), and

proposed the following equation:

$$B = C_B \left\{ 1.6 - 0.12 \ln(H_0 / L_0) + 0.28 \ln(\tan \beta) \right\}, \tag{3}$$

where H_0 is the wave height in deep water, and C_B is a nondimensional coefficient introduced with the consideration of scale effect.

The wave height-water depth ratio at wave reforming H_r/h_r is set to be 0.35 based on field data obtained by Kuriyama and Ozaki (1996).

When a significant wave height and a period are given at an offshore boundary, a time series of water surface elevation for ten minutes having the JONSWAP type spectrum at the offshore boundary is numerically simulated with the given wave height and period. Then, with the zero-down crossing method, the time series is divided into individual waves, which are used in the calculation.

The incident directions of individual waves at the offshore boundary are determined with the given principal wave direction, the directional spreading function of Mitsuyasu-type and the spreading parameter estimated with the method of Goda and Suzuki (1975). When the spreading parameter exceeds 100, the individual waves are treated as uni-directional waves.

The root-mean-square wave height H_{rms} and the wave height H_{m0}, which are defined with the root-mean-square of water surface elevation η_{rms} by

$$H_{rms} = 2\sqrt{2} \, \eta_{rms} \, , \tag{4}$$

$$H_{m0} = 4.004 \, \eta_{rms} \, , \tag{5}$$

are not directly estimated in the wave-by-wave approach. The values of H_{rms} and H_{m0}, thus, are obtained with the relationship between $H_{1/3}/\eta_{rms}$ and a dimensionless parameter $\Pi_{1/3}$, which has been propose by Goda (1983) for expressing wave nonlinearity. The parameter $\Pi_{1/3}$ is expressed by Eq.(6), and the relationship between $H_{1/3}/\eta_{rms}$ and $\Pi_{1/3}$, which has been obtained by Kuriyama (1996), is expressed by Eq.(7).

$$\Pi_{1/3} = H_{1/3} / L_{1/3} \coth^3(2\pi h / L_{1/3}). \tag{6}$$

$$\begin{aligned} H_{1/3} / \eta_{rms} &= 0.349 \ln \Pi_{1/3} + 4.648, & \Pi_{1/3} &\geq 0.1, \\ H_{1/3} / \eta_{rms} &= 3.8, & \Pi_{1/3} &< 0.1. \end{aligned} \tag{7}$$

In all calculations in this study, to minimize the error in the prediction of undertow velocity caused by the error in the prediction of wave height, coefficients C_{br} and C_B in Eqs. (1) and (3) were determined so that the predicted significant wave heights fit the measured values.

3-2 Undertow model

Undertow velocity of an individual wave V_{ind} is estimated with the mass flux due to wave motion Q_w and that due to surface roller Q_r.

$$V_{ind} = (Q_w + Q_r) / d_{tr}, \qquad (8)$$

where d_{tr} is the distance between the wave trough level and the bottom, and is obtained as $d_{tr} = h - H/2$.

The mass flux due to wave motion Q_w is calculated with the wave celerity C, the water depth h, and the root-mean-square of water surface elevation of an individual wave ζ_{rms} by the following equation proposed by Svendsen (1984).

$$Q_w = (C / h) \zeta_{rms}. \qquad (9)$$

The value of ζ_{rms} is estimated with the consideration of wave nonlinearity. With the parameter Π expressing nonlinearity of an individual wave and data shown by Goda (1983), the relationship between ζ_{rms} and H was obtained; the parameter Π and the relationship obtained are expresses by

$$\Pi = H / L \ \coth^3(2\pi h / L), \qquad (10)$$

$$
\begin{aligned}
\zeta_{rms} &= 1/8H^2, & \Pi &< 0.15, \\
\zeta_{rms} &= (1.668 \log \Pi + 4.204)^{-2} H^2, & 0.15 &\leq \Pi < 3, \\
\zeta_{rms} &= 1/25H^2, & \Pi &\geq 3.
\end{aligned}
\qquad (11)
$$

In the estimation of Q_r, the vertical distribution of the time-averaged velocity shown in the middle of Figure 5 is assumed. In previously proposed models (e.g., Svendsen, 1984), the vertical distribution shown in the left of Figure 5 is assumed; the time-average velocity in the roller is equal to C. Although just behind the front of the roller, the cross-shore velocity near the wave trough level sharply changes from shoreward velocity equal to C to
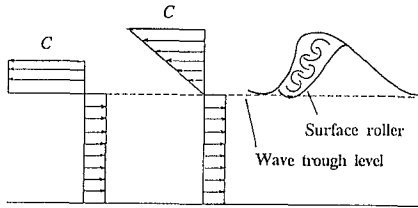
Figure 5   Vertical distribution of time-averaged
cross-shore current velocity assumed.

seaward undertow velocity, the cross-shore velocity in the middle of the roller is considered to change gradually from the top to the wave trough level. Hence, the vertical distribution shown in the middle of Figure 5 is assumed in the present model, and accordingly the mass flux due to the roller is obtained from

$$Q_r = A_r C / (2L),$$ (12)

where A_r is the area of the roller.

The area of the surface roller is estimated on the basis of two assumptions mentioned below.

1. The area of the surface roller fully developed is proportional to H^2.

2. Up to the point where the roller is fully developed, the roller develops without energy dissipation.

When the values of A_{r1} and A_{r2} are defined to be the roller areas obtained on the basis of the assumptions No.1 and No.2, respectively, the smaller value between A_{r1} and A_{r2} is assumed to be the area of the surface roller.

Even in the developing roller, some energy is dissipated. However, the amount of energy dissipation in the developing roller is considered to be smaller than that in the developed roller because turbulence in the developing roller is not fully developed. The amount of energy dissipation in the developing roller, hence, is assumed to be zero.

The area A_{r1} is estimated with a dimensionless coefficient C_A from

$$A_{r1} = C_A H^2.$$ (13)

The area A_{r2} is obtained from the following energy balance equation as Okayasu et al. (1990) and Dally and Brown (1995). In Eq.(14), however, the rate of energy dissipation is set to be zero.

$$\frac{\partial (E_w C_g)}{\partial y} + \frac{\partial (E_r C)}{\partial y} = 0,$$

$$E_r = \frac{1}{8} \rho C^2 \frac{A_{r2}}{L},$$ (14)

where E_r is the energy of the roller having the triangle-shaped distribution of the time-averaged velocity above the wave trough level.

4. Calibration

In the present model, C_A in Eq.(13) is a key coefficient for estimating the area of the surface roller. Hence, the model was calibrated with the field data of fourteen cases

obtained at HORS from 11 p.m. on January 30 to 10 a.m. on February 2 in 1997, when the wave heights were large.

The offshore boundary was set at P600m. The beach profiles measured every day were used for those shoreward of the tip of HORS, and the beach profile surveyed on January 16, 1997 shown in Figure 6 was used for that seaward of the tip of HORS; according to Kuriyama (1996), the amount of beach profile changes seaward of the tip of HORS is considered to be small.

The wave heights at the offshore boundary were estimated from the wave data obtained at a water depth of about 23m offshore of Kashima Port; the location of the wave gage is shown in Figure 1. The wave directions at the boundary were calculated with the Snell's law from the principal wave directions at P260m.

The value of C_A optimal for all cases was 7. The value of C_A optimal in each case, on the other hand, was related to the surf similarity parameter at the wave breaking position ξ_b. The parameter ξ_b is estimated by

$$\xi_b = \tan \beta \, / \, (H_{1/3,b} \, / \, L_{1/3,0})^{1/2} \, , \tag{15}$$

where $H_{1/3,b}$ is the significant wave height at wave breaking position and $L_{1/3,0}$ is the offshore wavelength corresponding to the significant wave period. The value of $H_{1/3,b}$ was defined to be the maximum of the significant wave heights over a longshore bar, and was obtained from the calculation result of wave transformation. The beach slope used in Eq.(15) was the value at the point where $H_{1/3,b}$ was defined.

Figure 7 shows the relationship between C_A optimal in each case and ξ_b. There is a positive correlation between them as Deigaard et al. (1991) and Dibajnia et al. (1994) reported; the correlation coefficient is 0.61. The value of C_A increased as ξ_b increased, that is, the coefficient increased as the ratio of the plunging breaker increased.
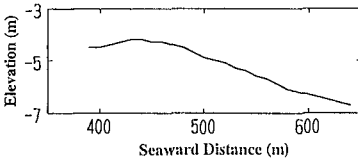
Figure 6   Beach profile seaward of the tip of
HORS surveyed on Jan. 16, 1997.
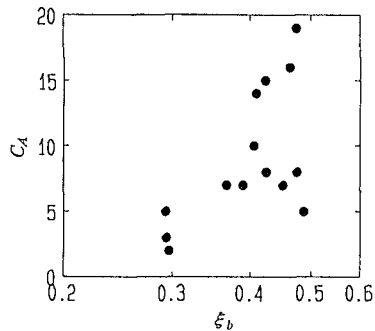
Figure 7   Relationship between C_A and ξ_b.

The relationship between C_A and ξ_b obtained with the least square method is given by

$$C_A = 17.0 \log \xi_b + 24.7 .\tag{16}$$

5. Comparisons of Models with Measurements

Undertow velocities predicted with C_A give by Eq.(16) and with $C_A=7$ were compared with the values measured in the field. Because ξ_b in the measurements ranged from 0.3 to 0.5, the values of C_A larger than 12 and those smaller than 4 were set to be 12 and 4, respectively. The values predicted with a model that has been proposed by Stive and De Vriend (1994) and calibrated by Reneirs and Battjes (1997) were also compared with the measurements; the model will be referred to as the previous model.

Figure 8 shows comparisons for four cases of the fourteen cases used in the calibration. The significant wave heights, periods, principal wave directions θ, water depths and mean water levels $\overline{\eta}$ at the offshore boundary, and ξ_b in the four cases are listed in Table 1; the values of s_{max} at the offshore boundary exceeded 100. As shown in Figure 8, the previous model, which has been calibrated with experiment data, underestimated the undertow velocities. Both models with C_A agreed with the measurements, while the performance of the model with C_A give by Eq.(16) was better than that of the model with the constant C_A.

The root-mean-square errors defined by

$$\varepsilon = \left(\frac{\sum (V_{meas} - V_{pred})^2}{\sum (V_{meas})^2} \right)^{1/2} ,\tag{17}$$

where V_{meas} and V_{pred} are the undertow velocities measured and predicted, for the fourteen cases used in the calibration were calculated for the three models. The values of ε for the previous model and the present models with $C_A =7$ and C_A give by Eq.(16) were 52%, 41% and 35%.

The models with C_A give by Eq.(16) and with $C_A =7$, and the previous model were also compared with the filed measurement of DELILAH (Smith et al., 1992) and the large-scale experiments of Delta Flume '93 (Rakha et al., 1996). The data on October 19, 1990 in DELILAH and of the cases 1-b and 1-c in Delta Flume '93 were used for the comparisons. The wave heights, periods, principal wave directions and water depths at the offshore boundaries are listed in Table 2, where T_p is the wave period at the spectral peak. The value of s_{max} exceeded 100 on October 19 in DELILAH.

Figure 9 shows a comparison of the models and the measurement DELILAH. Although the previous model underestimated the velocities, both of the models with C_A

Table 1   Offshore boundary conditions and ξ_b in measurements at HORS.

Case	$H_{1/3}$ (m)	$T_{1/3}$ (s)	θ	h (m)	$\bar{\eta}$ (m)	ξ_b
2	2.11	9.63	16.5	6.58	0.58	0.293
4	2.91	11.81	19.0	6.98	0.98	0.367
5	2.50	11.56	7.0	6.50	0.50	0.463
7	2.37	12.16	6.0	6.65	0.65	0.475
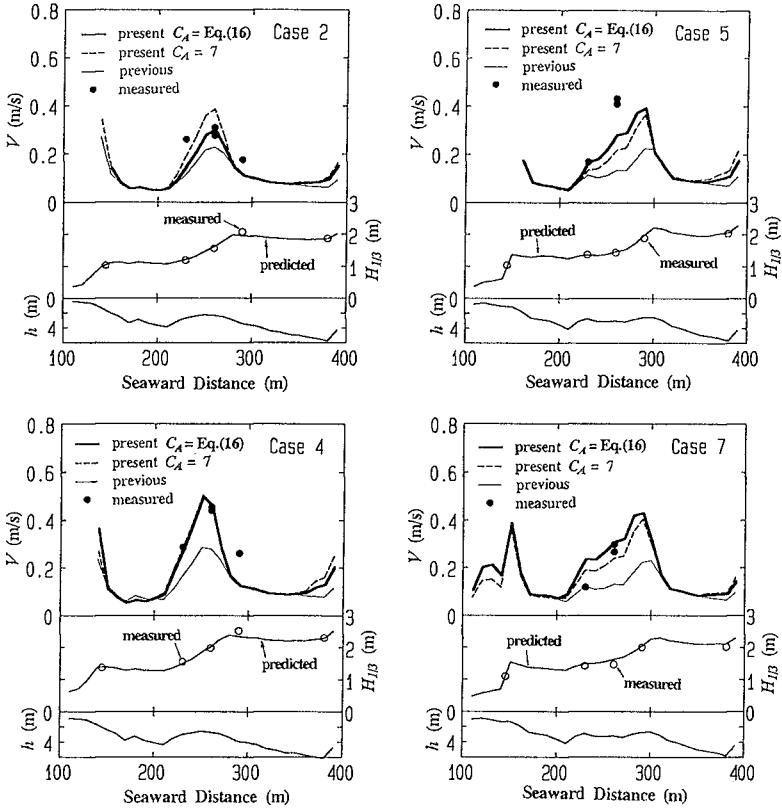
Figure 8   Comparisons of models with measurements at HORS.

Table 2   Offshore boundary conditions in
DELILAH and Delta Flume '93.

Case	H_{rms} (m)	T_p (s)	θ	H (m)
Oct. 19	0.75	7	15.1	2.63

Case	H_{m0} (m)	T_p (s)	h (m)
1b	1.40	5	4.1
1c	0.60	8	4.1
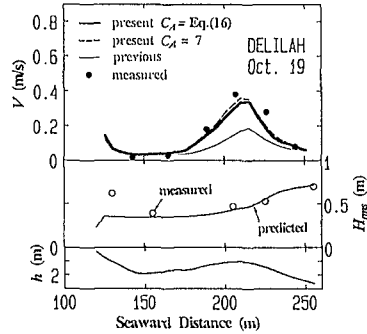
Figure 9   Comparisons of models with
DELILAH measurement.
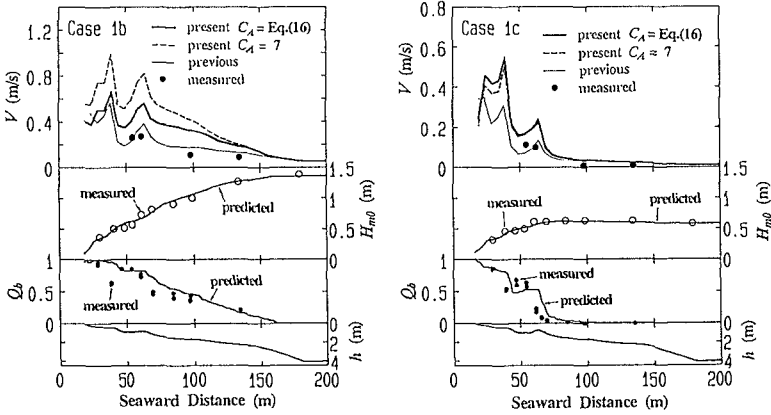
Figure 10   Comparisons of models with Delta Flume '93 experiments.

agreed with field data. Comparisons between the models and the measurements in Delta Flume '93 are shown in Figure 10. The previous model agreed with the measurements, while both models with C_A overestimated the undertow velocities. However, the performance of the model with C_A give by Eq.(16) was better than that of the model with the constant C_A.

6. Discussion

In the calibration of the present model of undertow, the time-averaged cross-shore
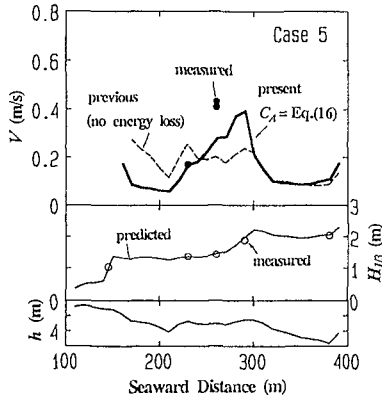
Figure 11   Comparisons of models with the
measurement in Case 5 at HORS.

velocity was assumed to be vertically uniform below the wave trough level, and the undertow velocities measured with one current meter at P230m and those at P290m were used. As shown in Figures 3 and 8, differences of the undertow velocities measured with two current meters at P260m were small, and this suggests that the assumption is appropriate.

Through the comparisons between the models and the measurements, it is concluded that for predicting undertow velocities over a longshore bar in the field where water depth ranges from 1 m to 3 m, the model with C_A give by Eq.(16) was better than that with C_A=7. The previous model, on the other hand, sometimes underestimated the undertow velocities in the field. Figure 11 shows a comparison between the undertow velocities measured in case 5 at HORS and those predicted with the present model having C_A give by Eq.(16) and with a modified previous model that assumes no energy dissipation. The previous model with no energy dissipation still underestimated the undertow velocities, and this result seems to suggest that the assumption of the rectangular-shaped distribution of time-averaged velocity above the wave trough level, shown in the left of Figure 5, is inappropriate. The previous model, however, has good agreements against experiment data (e.g., Dally and Brown, 1995). The discrepancy seems to be attributed to scale effect; size of vortex and the development of the surface roller in the field are considered to be different from those in small-scale experiments. For developing a model applicable to a wide range of conditions, from a small-scale experiment to the field, further improvement of the models and calibrations with a wide range of data would be required.

7. Conclusion

Field measurements of undertow were conducted over longshore bars at Hazaki Oceanographical Research Station (HORS), and the field data were used for the calibration of the one-dimensional model developed in this study. The calibration showed that the parameter C_A, which is the ratio of the area of the surface roller fully developed to the square of the wave height, had a positive correlation with the surf similarity parameter at the wave breaking position; the correlation is expressed by Eq.(16).

The field measurements, other field measurements and large-scale experiments were compared with one-dimensional models for undertow. The comparisons showed that the present model with C_A given by Eq.(16) well predicted the undertow velocities over the longshore bars, while a previous model calibrated with small-scale experiment data underestimated the velocities.

Acknowledgement

References

Deigaard, R., Justesen, P. and Fresoe J. (1991): Modelling of undertow by a one-equation turbulence model, *Coastal Eng.*, 15, pp.431-458.

Dibajnia, M., Shimizu, T. and Watanabe, A. (1994) : Profile change of a sheet flow dominated beach, *Proc. 24th Coastal Eng. Conf.*, ASCE, pp.1946-1960.

Dally, W.R. and Brown, C.A. (1995): A modeling investigation of the breaking wave roller with application to cross-shore currents, *J. Geophys. Res.*, Vol.100, No.C12, pp.24873-24883.

Goda, Y. and Suzuki, Y. (1975): Computation of refraction and diffraction of sea waves with Mitsuyasu's directional spectrum, *Tech. Note Port and Harbour Res. Inst.*, No.230, 45p. (*in Japanese*)

Goda, Y. (1983): A unified nonlinearity parameter of water waves, *Rep. Port and Harbour Res. Inst.*, Vol.22, No.3, pp.3-30.

Haines, J.W. and Sallenger, A.H., Jr. (1994) : Vertical structure of mean cross-shore currents across a barred surf zone, , *J. Geophys. Res.*, Vol.99, No.C7, pp.14223-14242.

Kuriyama, Y. and Ozaki, Y. (1996): Wave height and fraction of breaking waves on a bar-trough beach -Field measurements at HORS and modeling-, *Rep. Port and Harbour Res. Inst.*, Vol.35, No.1, pp.1-38.

Kuriyama, Y. (1996): Models of wave height and fraction of breaking waves on a barred beach, *Proc. 25th Coastal Eng. Conf.*, ASCE, pp.247-260.

Kuriyama, Y. (1996): Short-term cross-shore movements of longshore bars, *Proc. Coastal Eng.*, JSCE,

Vol.43, pp.576-580. (*in Japanese*)

McLellan, T.N. and Kraus N.C. (1991): Design guidance for nearshore berm construction, *Coastal Sediments '91*, ASCE, pp.2000-2011.

Okayasu, A., Shibayama, T., and Horikawa, K. (1988): Vertical variation of undertow in the surf zone, *Proc. 21st Coastal Eng. Conf.*, ASCE, pp.478-491.

Okayasu, A., Watanabe, A. and Isobe, M. (1990): Modeling of energy transfer and undertow in the surf zone, *Proc. 22nd Coastal Eng. Conf.*, ASCE, pp.123-135.

Okayasu, A. and Katayama, H. (1992): Distribution of undertow and long-wave component velocity due to random waves, *Proc. 23rd4 Coastal Eng. Conf.*, ASCE, pp.883-893.

Rakha, K.A., Deigaard, R., Madsen, P.A., Brøker, I. and Rønberg, J.K. (1996): Simulation of coastal profile development using a Boussinesq wave model, *Proc. 25th Coastal Eng. Conf.*, ASCE, pp.3048-3061.

Reniers, A.J.H.M. and Battjes, J.A. (1997): A laboratory study of longshore currents over barred and non-barred beaches, *Coastal Eng.*, 30, pp. 1-22,

Seyama, A. and Kimura, A. (1988): The measured properties of irregular wave breaking and wave height change after breaking on the slope, *Proc. 21st Coastal Eng. Conf.*, ASCE, pp.419-432.

Short, A.D. (1985): Rip-current type, spacing and persistence, Narrabeen Beach, Australia, *Marine Geology*, 65, pp.47-71.

Shuto, N. (1974): Nonlinear long waves in a channel of variable section, *Coastal Eng. Japan*, Vol.17, pp.1-12.

Smith, J.A. and Largier, J.L. (1995): Observations of nearshore circulation: Rip currents, *J. Geophys. Res.*, Vol.100, No.C6, pp.10967-10975.

Smith, J.M., Svendsen, I.A. and Putrevu, U. (1992): Vertical structure of the nearshore current at DELILAH: Measured and modeled, *Proc. 23rd Coastal Eng. Conf.*, ASCE, pp.2825-2838.

Stive, M.J.F. and Wind, H.G. (1986) : Cross-shore mean flow in the surf zone, *Coastal Eng.*, 10, pp.325-340.

Stive, M.J.F. and De Vriend, H.J. (1994): Shear stresses and mean flow in shoaling and breaking waves, *Proc. 24th Coastal Eng. Conf.*, ASCE, pp.594-607.

Svendsen, I.A. (1984): Mass flux and undertow in a surf zone, *Coastal Eng.*, 8, pp.347-365.

Svendsen, I.A. and Hansen, J.B. (1988) : Cross-shore currents in surf-zone modelling, *Coastal Eng.*, 12, pp.23-42.

Thornton, E.B. and Guza, R.T. (1983): Transformation of wave height distribution, *J. Geophys. Res.*, Vol.88, No.C10, pp.5925-5938.

Wright, L.D. and Short, A.D. (1983): Morphodynamics of beaches and surf zones in Australia, *CRC Handbook of Coastal Processes and Erosion*, edited by Komar, D., CRC Press Inc., pp.35-64.